Published in final edited form as:
J Bone Miner Res. 2012 September ; 27(9): 1936–1950. doi:10.1002/jbmr.1646.

Matrix Metalloproteinase-13 is Required for Osteocytic Perilacunar Remodeling and Maintains Bone Fracture Resistance

SY Tang[1], **R-P Herber**[2], **SP Ho**[3], and **T Alliston**[1,4]

[1]Department of Orthopedic Surgery, School of Dentistry University of California, San Francisco, CA 94143, USA

[2]Division of Orthodontics, Department of Orofacial Sciences, School of Dentistry University of California, San Francisco, CA 94143, USA

[3]Division of Biomaterials & Bioengineering, Department of Preventative & Restorative Dental Science, School of Dentistry University of California, San Francisco, CA 94143, USA

[4]Department of Bioengineering and Therapeutic Sciences, Department of Otolaryngology Head and Neck Surgery, Eli and Edythe Broad Center of Regeneration Medicine and Stem Cell Research, University of California, San Francisco, CA 94143, USA

Abstract

Like bone mass, bone quality is specified in development, actively maintained post-natally, and disrupted by disease. The roles of osteoblasts, osteoclasts, and osteocytes in the regulation of bone mass are increasingly well defined. However, the cellular and molecular mechanisms by which bone quality is regulated remain unclear. Proteins that remodel bone extracellular matrix, such as the collagen-degrading matrix metalloproteinase (MMP)-13, are likely candidates that regulate bone quality. Using MMP-13 deficient mice, we examined the role of MMP-13 in the remodeling and maintenance of bone matrix and subsequent fracture resistance. Throughout the diaphysis of MMP-13-deficient tibiae, we observed elevated nonenzymatic crosslinking and concentric regions of hypermineralization, collagen disorganization, and canalicular malformation. These defects localize to the same mid-cortical bone regions where osteocyte lacunae and canaliculi exhibit MMP-13 and tartrate-resistant acid phosphatase (TRAP) expression, as well as the osteocyte marker Sclerostin. Despite otherwise normal measures of osteoclast and osteoblast function, dynamic histomorphometry revealed that remodeling of osteocyte lacunae is impaired in MMP-13$^{-/-}$ bone. Analysis of MMP-13$^{-/-}$ mice and their wild-type littermates in normal and lactating conditions showed that MMP-13 is not only required for lactation-induced osteocyte perilacunar remodeling, but also for the maintenance of bone quality. The loss of MMP-13, and the resulting defects in perilacunar remodeling and matrix organization, compromise MMP-13$^{-/-}$ bone fracture toughness and post-yield behavior. Taken together, these findings demonstrate that osteocyte perilacunar remodeling of mid-cortical bone matrix requires MMP-13 and is essential for the maintenance of bone quality.

Corresponding Author: Tamara Alliston, PhD Associate Professor Department of Orthopedic Surgery University of California, San Francisco San Francisco, CA 94143 tamara.alliston@ucsf.edu.

Author roles: Study design: SYT and TA. Study conduct: SYT, RPH, SH, and TA. Data analysis; SYT, RPH, SH, and TA. Drafting of the manuscript: SYT, RPH, SH, and TA. Revising the manuscript content: SYT and TA. Approval of final version of the manuscript SYT and TA. SYT and TA take responsibility for the integrity of the data analysis.

Keywords

matrix metalloproteinase-13; bone matrix; osteocyte; remodeling; bone quality; fracture resistance; osteocyte perilacunar remodeling

Introduction

The ability of bone to resist fracture and provide mechanical support is critically derived from both the quantity and quality of the bone matrix, both of which must be actively maintained to respond to changing demands on this tissue [1]. Cortical bone quality encompasses many factors that span the hierarchical organization of bone, from cortical bone geometry at the macroscale [2,3], microdamage [4,5], and porosity [6,7] at the microscale, extracellular matrix material properties (i.e. elastic modulus and hardness) at the nanoscale [8,9], to collagen crosslinking [10–12] and mineral crystallinity and maturity [13] at the molecular scale. Each of these hierarchical relationships is biologically regulated and important for the overall function of bone [14–16]. For example, cochlear bone matrix is much harder than that of the femur [17,18], and the abnormal specification of these bone matrix material properties can impair bone-specific function – leading to hearing loss or fragility observed in genetically modified mice or human bone syndromes [18]. Likewise, defects in collagen crosslinking [19] or microdamage repair [20] have been implicated in fragility associated with disease and aging. While the importance of bone quality is clear, the mechanisms that establish, maintain, or disrupt it remain areas of active investigation.

Like bone mass, the maintenance of bone matrix quality requires the coordinated action of cells of both the osteoblast and osteoclast lineages. Osteoblast-specific mutations in the TGF–β type II receptor or heterozygous deletion of the osteoblast transcription factor Runx2 are sufficient to alter the elastic modulus of bone extracellular matrix. In contrast, inhibition of osteoclast-mediated bone remodeling by bisphosphonates increases mineral content of the bone matrix and the tissue elastic modulus, but reduces toughness [21,22]. In glucocorticoid treated mice, bone matrix mineralization and material properties are most profoundly affected in the perilacunar regions, suggesting a role for osteocytes [23]. Although the contribution of each cell type to bone mass is increasingly well-defined, the role of each cell type in regulating bone quality in response to changes in biological stimuli such as TGF–β and glucocorticoids (which can affect all three cell types) remains unclear. Also unknown are the specific proteins responsible for conferring changes in bone matrix quality in response to these signaling pathways.

When considering which proteins might participate in the active regulation of bone quality, matrix metalloproteinases (MMPs) emerge as strong candidates. MMPs remodel extracellular matrices throughout the body including bone [24]. The tight regulation of MMP expression and activity is essential for the development, maintenance, and repair of many tissues. Although the MMPs have redundant substrates (i.e., multiple MMPs cleave type I collagen) [25], the loss of even a single MMP can have adverse consequences on bone development. For example, mice deficient in membrane-type-1 (MT-1) MMP [26], MMP-2 [27], MMP-9 [28], and MMP-13 [29,30] have abnormal bone phenotypes, each arising from distinct mechanisms.

To explore mechanisms responsible for maintaining the quality of cortical bone matrix, we focused on MMP-13. This protease, expressed by cells of the chondrocyte and osteoblast lineages, degrades several substrates including collagen I, collagen II, and aggrecan [31]. In humans, missense mutations in the MMP-13 gene cause the skeletal disorder of spondyloepimetaphyseal dysplasia [32]. M M P-13 deficient mice have increased trabecular

bone volume at skeletal maturity [29,30]. Yet the role of MMP-13 in the regulation of cortical bone matrix quality is unclear. Several of the same factors known to regulate bone matrix material properties, including glucocorticoids, TGF-β, Smad3, and Runx2, also regulate the expression of MMP-13 [33–36]. Therefore, we hypothesize that MMP-13 remodeling of the cortical bone matrix is required to maintain bone quality.

To test this hypothesis, we examined the effects of systemic MMP-13 deletion on bone quality and on the cellular mechanisms thought to control it. The results show that the loss of MMP-13 reduces the fracture resistance of long bones, independently of changes in osteoclast-mediated bone resorption and osteoblast-mediated bone formation. While testing our hypothesis, these studies also uncovered a novel role for MMP-13 in remodeling of the osteocyte lacunar-canalicular network in cortical bone matrix, particularly in lactation. Together, these findings demonstrate the essential role of MMP-13 and perilacunar remodeling in the maintenance of bone quality.

Materials and Methods

Tibiae and femora were collected from euthanized two-month-old MMP-13$^{-/-}$ male mice and their wild-type (WT) littermates for analyses. The generation and phenotypes of these mice have been previously described [29,37]. Mice were maintained and treated in accordance with institutional animal care and use committee (IACUC)-approved protocols.

Histological Analysis

For all histological evaluation, the number of mice per genotype used for each assay (n) is given respectively. For each bone sample, at least 3 non-adjacent sections were examined.

Safranin-O staining (n=6)—Mouse tibiae from both WT and MMP-13$^{-/-}$ animals were collected, dissected free of soft-tissue, and fixed overnight in 4% paraformaldehyde in PBS at 4°C, prior to demineralization using a sodium-buffered solution of EDTA (final solution containing 0.24 M EDTA-2Na and 0.25 M EDTA-4Na) for 7 days at 4°C. Transverse 7 μm sections of paraffin-embedded tibiae were stained with a combination of hematoxylin, Safranin-O, and a Fast Green counter stain. To quantify the abundance of remnant growth plate cartilage within cortical bone, the Safranin-O positive regions were quantified by k-means segmentation using ImageJ (NIH) and expressed as a ratio relative to the total bone area in the section. This analysis was performed over the entire bone cross-section using images taken under a 10X objective.

Immunohistochemistry (n=3)—Immunohistochemical analysis of MMP-13 was performed on tibiae embedded in Tissue O.C.T. Compound (Sakura Finetek, CA, USA) for 10 μm frozen sections. MMP-13 localization was assessed using a goat-derived anti-mouse-MMP-13 primary antibody (AB-8012, Millipore, USA), which was detected with an HRP-conjugated donkey-anti-goat secondary antibody (SC-1012, Santa Cruz Antibodies, USA). Both the primary and secondary antibodies were diluted 1:200 in 1.5% donkey serum. A Vectastain Elite kit was used to perform DAB staining (Vector Labs; USA). Sclerostin expression was evaluated using primary goat anti-SOST antibody (AF 1589, R&D Systems, USA) with an anti-goat secondary antibody conjugated with HRP (Vectastain Elite ABC Goat IgG kit; Vector Labs; USA). The primary and secondary antibodies were diluted in 1.5% rabbit serum blocking buffer. Negative controls, including primary incubation with goat IgG and either anti-MMP-13 or anti-SOST, confirmed the specificity of the antibody staining.

Tartrate resistant acid phosphatase staining (n=4)—The activity of osteoclasts were assessed using a Leukocyte Acid Phosphatase kit with Fast Red Violet as the binding agent (Sigma-Aldrich, USA) on decalcified paraffinized sections with no counter staining. Osteoclast activity was measured along the periosteal and endosteal surfaces by identifying TRAP-positive cells following the published ASBMR conventions [38]. A k-means segmentation method using ImageJ was used to determine the percentage of TRAP-stained matrix relative to the total bone matrix area [39].

Thionin stain for the bone canalicular network (n=3)—The bone canalicular network was visualized by staining of decalcified frozen sections in a Thionin-based solution and then fixed in saturated picric acid [40,41].

Dynamic bone histomorphometry (n=5)—Mice were given two intraperitoneal injections of calcein (0.02 mg/g) five days apart prior to euthanasia. The tibiae were then collected and fixed in 4% paraformaldehyde in PBS, serially dehydrated in graded ethanol, and then embedded in a plastic resin (TechnoVit 5, EMS, Pennsylvania). The embedded blocks were sectioned using a tungsten carbide blade to a thickness of 8 μm and mounted on glass slides. The mineral apposition rate (MAR, mean inter-label thickness divided by the time between the two labelling periods) was computed at both the periosteal and the endosteal surface using ImageJ by evaluating fluorescent micrographs taken with a 20X optical objective. The bone formation rate (BFR) was calculated in accordance with the ASBMR nomenclature [38]. Calcein-labeled lacunae were quantified with the 40X optical objective over 3 non-adjacent sections for each animal. The number of calcein-labeled lacunae was normalized to the bone area, which was quantified using ImageJ.

Collagen Birefringence (n=3)—For polarized light microscopy of frozen sections, two polarized light filters were placed between the light path and the viewing objective. For each tissue section, the polarizing filters were rotated such that the maximum birefringence was achieved as confirmed by the resulting 10X image capture.

Structural and mineral composition analyses by microCT imaging

The tibiae (n=4) and femora (n=6) from both genotypes were used for microtomography analysis by the vivaCT 40 micro-computed tomography (microCT) system (Scanco Medical, Switzerland). The microCT imaging was conducted at a 9.5 μm isotropic voxel resolution. The trabecular bone compartment from six animals was evaluated by manual contouring over a 2 mm span distal to the tibial plateau (200 slices). From this region, the ratio of bone volume to total volume (BV/TV), trabecular connectivity (t.Conn), and the structural model index (SMI) were computed. To compute the trabecular bone tissue mineral density distribution, for each voxel over segmented and contoured slices, CT attenuation values were calibrated to a hydroxyapatite standard (mg HA/cm^3) and sorted into numerical bins. The final value was normalized by the total bone volume in the compartment.

The cortical bone compartment from the femur evaluated over a 3 mm span at the mid-diaphyseal region (300 slices). Dual semi-automated contours were used to outline the endosteal and periosteal surfaces. Cortical bone tissue mineral density was computed using a method similar to that used for trabecular bone. The average cortical thickness (c. Th.) and moment of inertia (MOI) were also computed. The mineral concentrations for the trabecular and cortical bone compartments were measured. Higher resolution x-ray microscopy scans were obtained using a MicroXCT-200 (Xradia Inc., Pleasanton, CA, USA). A 4x objective was used to obtain resolution of approximately 1.5 μm. X-rays were set to a peak voltage of 90 kVp and a power of 6 W. Each tomography was reconstructed from 3500 radiographic projections obtained from a full circle of 360°. Exposure times of 7 s were chosen to yield

6000 to 8000 counts per pixel of each recorded radiograph approximating 25% of the original X-ray intensity passing through the specimen and arriving at the detector. Associated tomographies were reconstructed using reconstruction software (XMReconstructor, Version 7.0.2817, Xradia Inc., Pleasanton, CA, USA). 3D images were post processed using the Xradia 3D viewer. In addition to these high-resolution analyses of bones from 2-month old mice, tibiae from 2, 4, 6, 14, 22, and 30-week old mice (n=2 for each time point) were assessed using high-resolution microCT X-ray microscopy.

Nonenzymatic crosslinking of the organic bone matrix (n=6)

Nonenzymatic glycation (NEG) of collagen results in the formation of advanced glycation end-products (AGEs) and has been associated with changes in bone remodeling and the loss of toughness and fracture resistance in bone [10,11]. A fluorimetric assay was used to evaluate the accumulation of AGEs in bone. The mid-shafts of mechanically tested femora were demineralized using EDTA for approximately 7 days at 4°C, and demineralization was confirmed using contact radiographs. The demineralized bone samples were then hydrolyzed using 6N HCl (24 hr, 110°C). AGEs content was determined from fluorescence readings taken using a SpectraMax M5 spectraphotometer (Molecular Devices; Sunnyvale, CA) at the excitation wavelength of 370 nm and emission wavelength of 440 nm. These readings were standardized to a quinine sulfate standard and then normalized to the amount of collagen present in each sample. The amount of collagen for each bone sample was computed based on the amount of hydroxyproline as determined using a chloramine-T colorimetric assay [42] that recorded the absorbance of the digested samples against a commercially available standard.

Biochemical analysis of dynamic bone resorption (n=9)

In vivo bone resorption was measured quantitatively using a commercial immunoassay for total deoxypyridinoline (DPD) (Quidel Inc, CA). DPD is a mature crosslink of type I collagen, formed by the enzymatic action of lysyl oxidase, that is released during bone resorption and is detectable in urine and plasma [43,44]. Urine samples were collected from both genotypes. The samples were collected in the morning from all mice over 3 non-consecutive days when the mice were 8 weeks old. Briefly, the urine samples were hydrolyzed, and then the lysates were allowed to bind to a monoclonal anti-DPD antibody to produce a colorimetric reaction that is normalized to a known standard of DPD. The DPD measurements were further normalized by the urinary levels of creatinine. The same urine hydrolysates were also assayed for hydroxyproline, another marker of tissue metabolism [43], and normalized to creatinine levels.

Effects of MMP-13 on Lactation mediated bone loss

Two-month-old MMP-13$^{-/-}$ and WT (n=4) female mice were allowed to become pregnant by mating with a WT male. Upon delivery of the pups, the litter size was adjusted to 8 pups, and the dams were switched to a 0.2% calcium/0.53% phosphorous feed (5TZ8 Lower calcium feed, TestDiet Corporation, MN) *ad libitum* in order to exacerbate the effects of lactation-mediated bone loss (Standard mouse feed contains 0.61% calcium/0.57% phosphorous). At day 14, the dams were sacrificed and the tibiae were harvested for microCT analyses as described above (vivaCT 40, Scanco Medical, Switzerland). Age-matched virgin MMP-13$^{-/-}$ and WT female mice (n=2) were used as nulliparous controls.

Analysis of gene expression

Tibiae from MMP-13$^{-/-}$ (n=7) and WT (n=5) 2 month old male mice were dissected, the proximal and distal ends were cut off, the marrow was flushed using a pressurized water jet containing PBS, and the surfaces were stripped of all soft tissues. Tibiae were pulverized

with a liquid nitrogen-cooled mortar and pestle, and added to TRIzol (Invitrogen, Carlsbad, CA) for RNA extraction and purification using the Invitrogen PureLink RNA Mini Kit. cDNA was synthesized from up to 1μg of RNA using the iScript cDNA Synthesis kit (Bio-Rad 170–8891), after which gene expression was assessed using SYBR-based qRTPCR with the following primers: L19 F-(ACGGCTTGCTGCCTTCGCAT), R-(AGGAACCTTCTCTCGTCTTCCGGG); OPG F-(AGAGCAAACCTTCCAGCTGC); OPG R-(CTGCTCTGTGGTGAGGTTCG); RANKL-F (CACCATCAGCTGAAGATAGT), RANKL-R (CCAAGATCTCTAACATGACG). Gene expression was normalized to the expression of RP-L19. Fold-induction was calculated using the delta-delta-CT method.

Mechanical Testing

We focused on cortical bone because trabecular bone fragility is critically dependent on BV/TV and architecture, as well as the bone matrix material properties, and thus the mechanistic cause of fragility at the whole bone level would not be discernable. Instead, we examined the cortical bone where we have verified that the geometric and structural properties of the two genotypes are indistinguishable from each other, thus allowing us to focus on the role of MMP-13 on the matrix and tissue level fragility.

Microindentation of cortical bone tissue **(n=6)—**The tibiae from each genotype were used for dynamic microindentation. The bone tissues were encased in an epoxy resin and sectioned transversely proximally from the tibio-fibular junction (TFJ) using a low-speed diamond wafering saw. The exposed bone cross-sections were then serially polished under hydrated conditions to a particle size of 0.25 μm. After preparation, the samples were indented to a depth of 100 μm at a frequency of 2 Hz using a microindenter with a 90° conical indentation tip with a rounded 2 μm radius (BioDent 1000 TDI, Active Life Scientific, CA). Using a dissection microscope to identify the indentation sites, three regions were indented on each cross-section (periosteal, middle, endosteal), and 3 unique indentations were made within each region. The force-deformation data were collected during loading and unloading, and the elastic moduli were computed from the unloading slope using the Oliver-Pharr method [45,46].

Three-point bending of whole bone (n=6)—Femora from MMP-13$^{-/-}$ and WT mice were dissected free of soft tissue, wrapped in HBSS-soaked gauze, and stored in sealed plastic at −20° C prior to three-point bending and fracture toughness tests. Samples were thawed to room temperature in HBSS, and then loaded to fracture in a three-point bending configuration (lower span: 5 mm) using the Bose ELF 3200 mechanical load frame (Bose, Eden Prairie, MN) under hydrated conditions. The crosshead was displaced at a rate of 0.005 mm/s until the bone was fractured. The force and displacement data were collected, and the following parameters were determined: Structural stiffness (the slope of the linear region of the force-displacement curve), ultimate load (the maximum force recorded during the cross-head displacement), post-yield deflection (deflection that took place between the yield and ultimate points), and post-yield work-to-fracture (area under the force-displacement curve between the yield and ultimate points). The transition to yielding was calculated using an automated criterion (executed in MatLab) that is determined when the piecewise slope of the force-displacement curve has been reduced to 90% of the initial stiffness [47].

Fracture toughness of the notched femora (n=6)—Thawed and hydrated femora from WT and MMP-13$^{-/-}$ mice were notched using a razor blade followed by diamond polish to cut the bone mid-shaft through less than 1/3 of its diameter. The notch was placed on the anterior-lateral side and then loaded in 3-point bending to propagate the notched flaw using the Bose ELF 3200 system at a displacement rate of 0.001 mm/s [48,49]. The force-displacement data was collected during the crosshead movement. The fracture surface

morphology including the crack angles and cortical diameter were measured using the vivaCT 40 microtomography system (Scanco Medical, Switzerland). The fracture toughness, K_C, was calculated using the unstable cracking method for the propagation of a circumferential through-wall flaw in cylinders [48].

Statistical analyses

Statistics were performed using Minitab 14 (Minitab Inc. State College, Pennsylvania). t-tests were used to ascertain the differences between groups of normally distributed data. The Chi-square test was used to compare the differences between distributions. Mann-Whitney nonparametric tests were used for non-normally distributed data. Significance of comparisons is defined by p-values equal to or less than 0.05.

Results

Heterogeneous mineralization of MMP-13$^{-/-}$ cortical bone

As a first step in testing the hypothesis that MMP-13 participates in the maintenance of post-natal bone matrix quality, micro-computed tomography was used to evaluate the mineralization of wild-type and MMP-13$^{-/-}$ bone. Consistent with previous reports [29,30,50], micro-computed tomography (microCT) imaging revealed a 34% increase in the mean trabecular bone volume fraction (BV/TV) in 2 month old MMP-13$^{-/-}$ tibiae relative to their wild-type littermates ($p < 0.001$; t-test; Figure 1A, 1B, 1E). In addition, the mean trabecular tissue mineral density was increased in MMP-13$^{-/-}$ mice, which resulted in an altered distribution of tissue mineral density ($p < 0.001$; chi-square test; Figure 1F). Stickens, et al. showed that this increased trabecular bone volume results from MMP13 deficiency in growth plate chondrocytes during endochondral ossification [29].

MicroCT also revealed defects in MMP-13$^{-/-}$ cortical bone mineralization that were independent of bone size or geometry. The cortical bone from MMP-13$^{-/-}$ tibiae and femora showed no differences in cortical thickness or moment of inertia (Figures 1C, D, G, Table I). Although the mean cortical bone TMD was indistinguishable between wild-type and MMP-13$^{-/-}$ mice, the distribution of mineral density was significantly altered. Specifically, the MMP-13$^{-/-}$ mice exhibited elevated instances of both increased and reduced mineral densities in the cortical bone ($p < 0.001$; Chi-square test; Figure 1H). The decreased values of cortical bone TMD may be related to the abundance of Safranin-O-stained of growth plate cartilage remnants that preferentially localize to the proximal tibial cortical bone of MMP-13$^{-/-}$ mice (Figures 1I, 1J). These osteoid remnants may explain the areas of hypomineralized MMP13$^{-/-}$ bone matrix [29,30], but do not explain the areas of increased mineral density.

Hypermineralization, collagen disorganization, and impaired turnover of MMP-13$^{-/-}$ bone matrix

To further investigate the increased proportion of hypermineralized bone in MMP13$^{-/-}$ mice, tibiae were scanned using higher resolution microCT. Reconstructed images of the tibia revealed a ring of hypermineralized matrix midway between the endosteal and periosteal surfaces of MMP-13$^{-/-}$ cortical bone that was not observed in wild-type littermates. This irregular ring of hypermineralization (Figures 2 A, B, E, F) spans longitudinally throughout the mid-diaphyseal region (Figures 2C, 2D). These data suggest that MMP13 plays a critical role in maintaining the normal distribution of mineral density in cortical bone.

Because the loss of MMP-13 has been associated with altered endochondral ossification [29], high resolution microCT was used to evaluate the dynamics of matrix

hypermineralization in MMP-13$^{-/-}$ mice and their WT littermates at 2-, 4-, 6- 9-, 14-, 22-, and 30- weeks old. Hypermineralization of the mid-cortical bone is apparent as early as two weeks of age. However, unlike other developmental aspects of the MMP-13$^{-/-}$ phenotype (i.e. the increased trabecular bone volume [29]), the ring of hypermineralization persists in 30 week old mice and increases in diameter such that it consistently remains approximately midway between the periosteum and endosteum. While this result does not preclude a developmental role for MMP-13 in hypermineralization, it suggests that MMP-13 also regulates bone matrix mineralization post-natally.

The abnormal mineralization of MMP-13 cortical bone raised questions about the organization of the organic components of bone matrix. Whereas polarized microscopy of WT cortical bone matrix showed birefringent lamellar bands that were concentric to the radial axis of the bone, this organization was disrupted in MMP-13$^{-/-}$ bone. Although the lamellar collagen birefringence near the endosteal and periosteal surfaces was fairly normal (not shown), collagen birefringence of MMP-13$^{-/-}$ bone was perturbed in the same mid-cortical regions where hypermineralization was observed (Figures S1 A, B, C, D).

The aberrant collagen organization suggested a defect in matrix remodeling. To determine the effect of MMP-13-deficiency on bone matrix remodeling, WT and MMP13$^{-/-}$ tibiae was assayed to determine the extent of collagen nonenzymatic glycation, a crosslink that accumulates over time such that it is elevated in unremodeled bone [10]. The level of nonenzymatic glycation was significantly increased in the MMP-13$^{-/-}$ bone relative to WT ($p < 0.05$; t-test; Figure S1E). This result suggests that MMP13 is required for post-natal bone matrix turnover. Furthermore, since accumulation of advanced glycation end-products (AGEs) reduces the ability of the individual collagen fibrils to deform and dissipate energy [12], the highly cross-linked MMP-13$^{-/-}$ bone matrix may have impaired material properties.

Normal measures of osteoclast and osteoblast function in MMP-13$^{-/-}$ bone

Defects in bone matrix remodeling typically reflect a loss of osteoclast activity. The effect of MMP-13-deficiency on osteoclast mediated bone remodeling has not been definitively examined, despite reports that MMP-13 is expressed by bone lining cells in areas of osteoclast activity [51,52]. To better understand the role of MMP-13 in bone turnover, several other measures of tissue and bone remodeling were assessed. As expected, the global loss of MMP-13 significantly impaired systemic collagen turnover, shown by the decreased urinary excretion of hydroxyproline ($p < 0.05$; t-test; Figure 3A). However, the levels of urinary deoxypyridinoline revealed no significant differences in bone-specific collagen turnover between the WT and MMP-13$^{-/-}$ mice (Figure 3B). Histological evaluation of tartrate resistant acid phosphatase (TRAP) activity, a key enzyme for osteoclast-mediated bone resorption, showed no differences in the number of TRAP-positive multinucleated osteoclasts between the WT and MMP-13$^{-/-}$ bone (Figures 3 C, I, J). Though the osteoclasts were primarily present on the endosteal and periosteal surfaces of cortical bone, we also observed strong TRAP-positive staining of mid-cortical bone. This irregular ring of TRAP staining did not correspond to multi-nucleated TRAP-positive osteoclasts and was not different between the two genotypes (Figures 3 D, G, H). Although TRAP expression is commonly associated with osteoclast activity, it has also been observed that osteocytes express TRAP to facilitate osteocyte-mediated bone remodeling in a process referred to as osteocytic osteolysis [53]. The lack of detectable differences in markers of bone turnover, osteoclast number, or TRAP staining was consistent with the results of dynamic bone histomorphometry, which also showed no differences in the rate of bone deposition, a process that is normally coupled to osteoclast-mediated bone turnover (Figures 3 E, F, K, L, M, N). Nor did mRNA levels for osteoclast-regulatory factors RANKL or OPG differ between bone from WT and MMP-13$^{-/-}$ mice (data not shown). Therefore, MMP13-

deficiency causes defects in cortical bone matrix composition and organization even when cortical bone remodeling by osteoclasts is intact and functioning normally. This led us to investigate where in the cortical bone matrix MMP-13 is normally expressed and which cell type might be responsible for the observed matrix disorganization.

A role for MMP-13 in remodeling of mid-cortical bone

We tested the hypothesis that defects in MMP-13$^{-/-}$ cortical bone matrix colocalized with the normal expression pattern of MMP-13. Immunohistochemical analysis revealed a distinctive ring of intense peri-lacunar MMP-13 expression that spreads throughout the mid-cortex of diaphyseal tibial bone (Figure 4A, B). As expected, similar regions in the MMP13−/− mouse bones did not express MMP-13 (Figure 4G, H). Together with the undetectable staining in wild-type bone incubated with a control IgG instead of anti-MMP-13 (Figure 4I, J), these data confirm the specificity of this unique pattern of MMP-13 expression in post-natal mid-cortical bone matrix. This gross staining pattern did not colocalize with any specific morphological features (Figure 4 C, D, E, F).

Higher magnification analysis reveals that MMP-13 protein is present within the osteocyte lacunae and canaliculi that spread throughout the bone matrix (Figure 5A). This staining pattern resembles that of SOST, another osteocyte-derived protein (Figure 5B). Furthermore, the region of highest expression of MMP-13 overlaps with the area of intense TRAP-positive cortical bone matrix (Figure 5E, F). Thionin staining of MMP-13−/− bone matrix reveals that the osteocyte-lacunar-canalicular network is disrupted, most severely in the midcortical bone matrix (Figure 5C, D) that corresponds to the defects in collagen organization and mineralization in MMP-13−/− mice (Figure 5G, 5H).

Calcified bone sections from the calcein-injected mice reveal that WT osteocytes regularly incorporate the fluorochrome in lacunae (Figure 5I), a phenomenon that is virtually absent in the MMP-13-deficient bone (Figure 5J). In addition, the intensity of fluorochrome labeling is noticeably greater in the WT osteocytes than the MMP-13 deficient osteocytes in the midcortical bone region (Figure 5K, L). Quantitative analysis of labeled lacunae in the entire bone section confirms that osteocyte perilacunar bone matrix remodeling in impaired throughout the MMP-13-deficient bone (Figure 5M).

Loss of MMP-13 reduces lactation-induced osteocyte perilacunar matrix remodeling

We next sought to determine if MMP-13-deficiency impacted osteocyte perilacunar remodeling during lactation, a physiological condition that drives osteocyte osteolysis to meet the elevated calcemic and phosphate demands. During lactation, tibial cortical bone porosity and endosteal perimeter increased (Figure 6 A, B)), whereas bone area and tissue mineral density decreased, relative to tibiae from nulliparous mice (Figure 6 C–F). In contrast, tibiae from lactating MMP-13-deficient mice exhibited small and non-significant changes (compared to MMP-13$^{-/-}$ nulliparous animals) in these same measured parameters. These results suggest that MMP-13 contributes to lactation-induced bone loss, and that MMP-13-deficiency hampers the ability of osteocytes to remodel the perilacunar bone matrix.

Loss of MMP13-mediated cortical bone remodeling compromises bone quality

Osteocyte-mediated cortical bone turnover has previously been implicated in the maintenance of mineral homeostasis during lactation, hibernation, and embryo development [54, 68]. However its role in the maintenance of post-natal bone quality has not been described. We hypothesize that loss of cortical bone remodeling in MMP-13$^{-/-}$ mice may impair bone quality, despite normal mean tissue mineral density and geometry. Microindentation was used to evaluate the material quality of bone matrix. The average

values of elastic modulus at the tissue level were similar between WT and MMP-13 bone matrix (Figure 7A) but the site-to-site variability within each bone was notably higher in MMP-13$^{-/-}$ mice (Figure 7B). This increased variability in material properties mirrors the variability in mineral density (Figure 1H). MMP-13$^{-/-}$ mice also showed increased cortical bone fragility through reduced post-yield work-to-fracture ($p < 0.001$; t-test; Figure 7C, 7D) and post-yield deflection ($p < 0.001$; t-test; Figure 7E). Although other parameters including whole bone structural stiffness and ultimate load did not exhibit differences between the MMP-13$^{-/-}$ and WT mice (Table II), the post-yield parameters measured here reflect a decreased capacity for MMP-13$^{-/-}$ bone to resist catastrophic fracture through toughening mechanisms. The lack of difference in the structural aspects of cortical bone, and the loss of whole bone fracture resistance suggest that the material properties of the MMP-13$^{-/-}$ bone extracellular matrix may be altered independently of bone geometry. Indeed, fracture toughness, a tissue-level material property, was significantly reduced in the MMP-13 deficient animals ($p < 0.001$; Figure 7F). Therefore, loss of MMP-13-mediated cortical bone remodeling impairs bone matrix composition, organization, and function.

Discussion

Here we show that osteocytic perilacunar remodeling of cortical bone by MMP-13 is essential for the maintenance of normal bone matrix composition, organization and fracture resistance. Even without detectable changes in osteoclast-mediated bone resorption, MMP-13 deficiency impairs cortical bone remodeling, resulting in canalicular abnormalities, hypermineralization and disorganization of the collagen-rich cortical bone matrix, in part due to failure to remodel the bone matrix around the osteocyte lacunae. Together, these defects are responsible for the fragility of MMP-13 deficient bone. These data suggest an essential role for MMP-13 and perilacunar bone matrix remodeling in the active maintenance of bone quality.

Loss of MMP-13 significantly reduces the fracture resistance of bone. This increased fragility likely reflects the combined effects of multiple mechanisms operating at different length scales. Fragility is not due to macroscale changes in cortical bone mass or geometry, neither of which are affected by MMP-13-deficiency. At the micron scale, collagen disorganization in the mid-cortical bone matrix localizes to the regions that normally express the highest levels of MMP-13 (Figures 3, 5). Other defects in collagen organization, such as those resulting from collagen point mutations in osteogenesis imperfecta, are well known to account for bone fragility [55]. The band of hypermineralized matrix in the same mid-cortical region of MMP-13 deficient bone may also compromise fracture toughness by creating abrupt interfaces that become stress risers [56]. Such sharp changes in material properties of bone can increase microcrack initiation and propagation [57], which can in turn predispose these regions for catastrophic failure. Accordingly, microindentation confirmed the heterogeneity of bone matrix material properties that corresponds to the abnormal bone matrix mineralization.

Normally, the material quality of bone matrix is actively maintained and regulated to accommodate changing mechanical or nutritional demands. Several known regulators of bone matrix material properties including glucocorticoids [16] and transforming growth factor β (TGF-β), also regulate MMP-13 expression. Therefore, it is possible that TGF-β and glucocorticoids exert some of their effects on bone matrix material properties through MMP-13, undoubtedly in cooperation with several other factors through mechanisms that remain to be identified. At the molecular scale, MMP-13$^{-/-}$ bone matrix has increased levels of nonenzymatic crosslinks. The accumulation of nonenzymatic crosslinks, which occurs normally with aging [11] and with reduced osteoclast-mediated bone remodeling [21], reduces the ability of bone to effectively dissipate energy to resist fracture [19,58–60].

Consequently, the increased crosslinking of collagen in MMP-13 deficient bone matrix is very likely another mechanism contributing to the reduced fracture toughness of these bones [60]. Because we measured nonenzymatic crosslinking in the entire midshaft, containing both normal and abnormal regions of the MMP-13$^{-/-}$ bone, the organic modifications in the MMP-13-deficient bone matrix are likely greater than what we observed. These changes in the organic components may also impact the functional mineralization of bone matrix quality, best assessed at a scale equivalent to the dimension of basic constituents that would identify changes in collagen crosslinks, intra- and extra-fibrillar mineral. The multi-scale analyses here suggest that MMP-13-mediated remodeling of the cortical bone matrix is required to maintain bone quality at the macro, micro, nano, and molecular length scales.

Other MMPs have also been shown to critically contribute to bone function and metabolism. In particular, a recent study by Nyman, et al. showed that deficiency in MMP-2 or MMP-9 also disrupts bone quality at several length scales – ultimately compromising the macro-mechanical behavior of MMP-2$^{-/-}$ and MMP-9$^{-/-}$ bone [28]. Since both MMP-2 and MMP-9 are cleaved and activated by MMP-13 [27,61], some of the defects in MMP-13$^{-/-}$ mice may reflect loss of function in MMP-2 and MMP-9. However, the mechanisms by which MMP-2, MMP-9 or MMP-13-deficiency impair overall bone quality are quite unique. For example, only MMP-13$^{-/-}$ mice exhibit defective macro-mechanical properties independently of macro-scale changes in cortical bone. This suggests that each MMP plays a non-redundant role in the maintenance of bone quality [28]. This conclusion is supported by studies of MT1-MMP and MMP-2 deficient mice [26,27], which showed malformation of the osteocyte lacunar-canalicular network, consistent with our findings here in MMP-13$^{-/-}$ mice. MT1-MMP$^{-/-}$ mice have canalicular disruptions in both long and parietal bones, while MMP-2$^{-/-}$ mice show differential defects in long and parietal bones. Whether or not the loss of MMP-13 affects the canalicular network in a manner that is anatomically distinct remains to be determined. While in MMP9$^{-/-}$ mice these defects are accompanied by abnormalities in osteoclast mediated matrix remodeling, others (MMP2$^{-/-}$, MMP-13$^{-/-}$) have apparently normal osteoclast function [27]. Together these studies demonstrate that the cell-type specific and spatially-distinct expression pattern of multiple MMPs is required for local turnover of bone matrix that maintains the osteocyte lacunar-canalicualar network and bone quality.

Several lines of evidence support a role for MMP-13 in osteocyte-mediated bone remodeling, or osteocytic osteolysis. Osteocytic osteolysis was first described in extenuating physiological circumstances such as lactation [62–64,69], and hibernation [65–67], in which osteocytes locally resorb the perilacunar matrix to maintain mineral homeostasis. Qing, *et al* recently demonstrated that osteocytes can express genes associated with osteoclastic remodeling to directly modify the perilacunar matrix [68]. Moreover, during physiological events such as lactation, the expression of these genes – as well as of MMP-13 – increases together with cortical bone porosity, further suggesting a role for the osteocyte-mediated resorption of bone matrix [68]. This is consistent with our findings that TRAP and MMP-13 are present at high levels in midcortical bone matrix, as well as the defect in lactation-induced osteocyte perilacunar remodeling in MMP-13$^{-/-}$ mice. It is worth nothing that the lactation model used here may be confounded by hyperparathyroidism since the lactating animals also received a low calcium diet. Nevertheless, our results demonstrate that the loss of MMP-13 has significant consequences on the local remodeling of cortical bone, causing disruption of the osteocyte lacunar-canalicular network, abnormal collagen and mineral organization, and reduced bone quality. Together, these findings suggest that MMP-13 and osteocyte perilacunar bone remodeling is essential for normal bone maintenance. This work has significant implications for understanding the osteocyte perilacunar changes and fragility that accompany glucorticoid-induced osteoporosis [16], especially since glucorticoids can regulate MMP-13 expression [16]. Additional study is needed to better

understand the mechanisms by which osteocytes maintain the quality of bone matrix and by which this process is disrupted in disease.

Supplementary Material

Refer to Web version on PubMed Central for supplementary material.

Acknowledgments

The authors gratefully acknowledge Dr. Sylvain Provot and Professor Zena Werb for the MMP-13$^{-/-}$ mice and Drs. Mary Beth Humphrey, Mary Nakamura, and Larry Suva for helpful scientific discussion. The authors also gratefully acknowledge Eunice Fu, Daniel Nguyen, Jacqueline Nguyen, and Ellora Berthet for technical assistance. This study was supported by NIH: F32AR059497 (ST) and R01DE019284 (TA). Support was also provided by Department of Orofacial Sciences, Division of Orthodontics, and Department of Preventive and Restorative Dental Sciences, UCSF, and NCRR/NIH S10RR026645 (SPH).

References

[1]. Hernandez CJ, Keaveny TM. A biomechanical perspective on bone quality. Bone. 2006; 39:1173–1181. [PubMed: 16876493]

[2]. Faulkner KG, Cummings SR, Black D, et al. Simple measurement of femoral geometry predicts hip fracture: The study of osteoporotic fractures. J Bone Min Res. 1993; 8:1211–1217.

[3]. Beck TJ, Ruff CB, Bissessur K. Age-related changes in female femoral geometry: implications for bone strength. Calcif Tiss Int. 1993; 53:S41–S46.

[4]. Vashishth D, Behiri JC, Bonfield W. Crack growth resistance in cortical bone: concept of microcrack toughening. J Biomech. 1997; 30:763–769. [PubMed: 9239560]

[5]. Diab T, Vashishth D. Effects of damage morphology on cortical bone fragility. Bone. 2005; 37:96–102. [PubMed: 15897021]

[6]. Burghardt AJ, Kazakia GJ, Ramachandran S, et al. Age and gender related differences in the geometric properties and biomechanical significance of intra-cortical porosity in the distal radius and tibia. J Bone Miner Res. 2009; 25:983–993. [PubMed: 19888900]

[7]. Tang SY, Vashishth. The relative contributions of non-enzymatic glycation and cortical porosity on the fracture toughness of aging bone. J Biomech. 2011; 44:330–336. [PubMed: 21056419]

[8]. Silva MJ, Brodt MD, Fan Z, Rho J-Y. Nanoindentation and whole-bone bending estimates of material properties in bones from the senescence accelerated mouse SAMP6. J Biomech. 2004; 37:1639–1646. [PubMed: 15388305]

[9]. Balooch G, Balooch M, Nalla RK, et al. TGF-beta regulates the mechanical properties and composition of bone matrix. Proc Natl Acad Sci. 2005; 102:18813–18818. [PubMed: 16354837]

[10]. Vashishth D, Gibson GJ, Khoury JI, et al. Influence of nonenzymatic glycation on biomechanical properties of cortical bone. Bone. 2001; 28:195–201. [PubMed: 11182378]

[11]. Wang X, Shen X, Li X, Agrawal CM. Age-related changes in the collagen network and toughness of bone. Bone. 2002; 31:1–7. [PubMed: 12110404]

[12]. Zimmermann EA, Schaible E, Bale H, et al. Age-related changes in the plasticity and toughness of human cortical bone at multiple length scales. Proc Natl Acad Sci. 2011; 108:14416–14421. [PubMed: 21873221]

[13]. Boskey AL, DiCarlo E, Paschalis E, et al. Comparison of mineral quality and quantity in iliac crest biopsies from high- and low-turnover osteoporosis: an FTIR microspectroscopic investigation. Osteopor Int. 2005; 16:2031–2038.

[14]. Li CY, Schaffler MB, Wolde-Semait HT, et al. Genetic background influences cortical bone response to ovariectomy. J Bone Miner Res. 2005; 20:2150–2158. [PubMed: 16294268]

[15]. Mohammad KS, Chen CG, Balooch G, et al. Pharmacologic inhibition of the TGF-beta type I receptor kinase has anabolic and anti-catabolic effects on bone. PLoS ONE. 2009; 4:e5275. [PubMed: 19357790]

[16]. Lane NE, Yao W. Glucocorticoid-induced bone fragility. Ann N Y Acad Sci. 2010; 1192:81–83. [PubMed: 20392221]

[17]. Currey JD. The design of mineralised hard tissues for their mechanical functions. J Exp Biol. 1999; 202:3285–3294. [PubMed: 10562511]

[18]. Chang JL, Brauer DS, Johnson J, et al. Tissue-specific calibration of extracellular matrix material properties by transforming growth factor-β and Runx2 in bone is required for hearing. EMBO Rep. 2010; 11:765–771. [PubMed: 20847738]

[19]. Tang SY, Zeenath U, Vashishth D. Effects of non-enzymatic glycation on cancellous bone fragility. Bone. 2007; 40:1144–1151. [PubMed: 17257914]

[20]. Burr DB, Martin RB, Schaffler MB, Radin EL. Bone remodeling in response to in vivo fatigue microdamage. J Biomech. 1985; 18:189–200. [PubMed: 3997903]

[21]. Tang SY, Allen MR, Phipps R, et al. Changes in non-enzymatic glycation and its association with altered mechanical properties following 1-year treatment with risedronate or alendronate. Osteopor Int. 2009; 20:887–894.

[22]. Allen MR, Iwata K, Phipps R, Burr DB. Alterations in canine vertebral bone turnover, microdamage acculumation, and biomechanical properties following 1-year treatment with clinical treatment doses of risedronate or aledronate. Bone. 2006; 39:872–879. [PubMed: 16765660]

[23]. Lane NE, Yao W, Balooch M, et al. Glucocorticoid-treated mice have localized changes in trabecular bone material properties and osteocyte lacunar size that are not observed in placebo-treated or estrogen-deficient mice. J Bone Miner Res. 2006; 21:466–476. [PubMed: 16491295]

[24]. Rundhaug JE. Matrix metalloproteinases and angiogenesis. J Cell Mol Med. 2005; 9:267–285. [PubMed: 15963249]

[25]. Krane SM, Inada M. Matrix metalloproteinases and bone. Bone. 2008; 43:7–18. [PubMed: 18486584]

[26]. Holmbeck K, Bianco P, Pidoux I, et al. The metalloproteinase MT1-MMP is required for normal development and maintenance of osteocyte processes in bone. J Cell Sci. 2005; 118:147–156. [PubMed: 15601659]

[27]. Inoue K, Mikuni-Takagaki Y, Oikawa K, et al. A crucial role for matrix metalloproteinase 2 in osteocytic canalicular formation and bone metabolism. J Biol Chem. 2006; 281:33814–33824. [PubMed: 16959767]

[28]. Nyman JS, Lynch CC, Perrien DS, et al. Differential effects between the loss of MMP-2 and MMP-9 on structural and tissue-level properties of bone. J Bone Miner Res. 2011; 26:1252–1260. d. [PubMed: 21611966]

[29]. Stickens D, Behonick DJ, Ortega N, et al. Altered endochondral bone development in matrix metalloproteinase 13-deficient mice. Development. 2004; 131:5883–5895. [PubMed: 15539485]

[30]. Inada M, Wang Y, Byrne MH, et al. Critical roles for collagenase-3 (Mmp13) in development of growth plate cartilage and in endochondral ossification. Proc Natl Acad Sci. 2004; 101:17192–17197. [PubMed: 15563592]

[31]. Nagase H, Woessner JF. Matrix metalloproteinases. J Biol Chem. 1999; 274:21491–21494. [PubMed: 10419448]

[32]. Kennedy AM, Inada M, Krane SM, et al. MMP13 mutation causes spondyloepimetaphyseal dysplasia, Missouri type (SEMD(MO). J Clin Invest. 2005; 115:2832–2842. [PubMed: 16167086]

[33]. Richardson DW, Dodge GR. Dose-dependent effects of corticosteroids on the expression of matrix-related genes in normal and cytokine-treated articular chondrocytes. Inflamm Res. 2003; 52:39–49. [PubMed: 12608648]

[34]. Johansson N, Westermarck J, Leppä S, et al. Collagenase 3 (matrix metalloproteinase 13) gene expression by HaCaT keratinocytes is enhanced by tumor necrosis factor alpha and transforming growth factor beta. Cell Growth Differ. 1997; 8:243–250. [PubMed: 9040946]

[35]. Tardif G, Reboul P, Dupuis M, et al. Transforming growth factor-beta induced collagenase-3 production in human osteoarthritic chondrocytes is triggered by Smad proteins: cooperation between activator protein-1 and PEA-3 binding sites. J Rheumatol. 2001; 28:1631–1639. [PubMed: 11469472]

[36]. Selvamurugan N, Jefcoat SC, Kwok S, et al. Overexpression of Runx2 directed by the matrix metalloproteinase-13 promoter containing the AP-1 and Runx/RD/Cbfa sites alters bone remodeling in vivo. J Cell Biochem. 2006; 99:545–557. [PubMed: 16639721]

[37]. Ortega N, Behonick DJ, Colnot C, et al. Galectin-3 is a downstream regulator of matrix metalloproteinase-9 function during endochondral bone formation. Mol Biol Cell. 2005; 16:3028–3039. [PubMed: 15800063]

[38]. Parfitt AM, Drezner MK, Glorieux FH, et al. Bone histomorphometry: standardization of nomenclature, symbols, and units. Report of the ASBMR Histomorphometry Nomenclature Committee. J Bone Miner Res. 1987; 2:595–610. [PubMed: 3455637]

[39]. Sawyer A, Lott P, Titrud J, McDonald J. Quantification of tartrate resistant acid phosphatase distribution in mouse tibiae using image analysis. Biotech Histochem. 2003; 78:271–278. [PubMed: 14989645]

[40]. Derkx P, Birkenhäger-Frenkel DH. A thionin stain for visualizing bone cells, mineralizing fronts and cement lines in undecalcified bone sections. Biotech Histochem. 1995; 70:70–74. [PubMed: 7578591]

[41]. Allison RT. Picro-thionin (Schmorl) staining of bone and other hard tissues. Br. J Biomed Sci. 1995; 52:162–164. [PubMed: 8520253]

[42]. Woessner JF. The determination of hydroxyproline in tissue and protein samples containing small proportions of this imino acid. Arch Biochem Biophys. 1961; 93:440–447. [PubMed: 13786180]

[43]. Garnero P, Delmas PD. New developments in biochemical markers for osteoporosis. Calcif Tissue Int. 1996; 59(Suppl 1):S2–9. [PubMed: 8974724]

[44]. Lenora, Ivaska, Obrant, Gerdhem. Prediction of bone loss using biochemical markers of bone turnover. Osteopor Int. 2007; 18:1297–1305.

[45]. Oliver W, Pharr G. Measurement of hardness and elastic modulus by instrumented indentation: Advances in understanding and refinements to methodology. J Mater Res. 2004; 19:3–20.

[46]. Tang SY, Mathews P, Randall C, et al. In situ materials characterization using the tissue diagnostic instrument. Polymer Testing. 2010; 29:159–163. [PubMed: 20582333]

[47]. Jepsen KJ, Pennington DE, Lee YL, Warman M, Nadeau J. Bone brittleness varies with genetic background in A/J and C57BL/6J inbred mice. J Bone Miner Res. 2001; 16:1854–1862. [PubMed: 11585350]

[48]. Ritchie RO, Koester KJ, Ionova S, et al. Measurement of the toughness of bone: a tutorial with special reference to small animal studies. Bone. 2008; 43:798–812. [PubMed: 18647665]

[49]. Vashishth D. Small animal bone biomechanics. Bone. 2008; 43:794–797. [PubMed: 18672104]

[50]. Behonick DJ, Xing Z, Lieu S, et al. Role of matrix metalloproteinase 13 in both endochondral and intramembranous ossification during skeletal regeneration. PLoS ONE. 2007; 2:e1150. [PubMed: 17987127]

[51]. Holliday LS, Welgus HG, Fliszar CJ, et al. Initiation of osteoclast bone resorption by interstitial collagenase. J Biol Chem. 1997; 272:22053–22058. [PubMed: 9268345]

[52]. Nakamura H, Sato G, Hirata A, Yamamoto T. Immunolocalization of matrix metalloproteinase-13 on bone surface under osteoclasts in rat tibia. Bone. 2004; 34:48–56. [PubMed: 14751562]

[53]. Aarden EM, Burger EH, Nijweide PJ. Function of osteocytes in bone. J Cell Biochem. 1994; 55:287–299. [PubMed: 7962159]

[54]. Bonewald L. The amazing osteocyte. J Bone Min Res. 2010; 26:229–238.

[55]. Kozloff KM, Carden A, Bergwitz C, et al. Brittle IV mouse model for osteogenesis imperfecta IV demonstrates postpubertal adaptations to improve whole bone strength. J Bone Miner Res. 2004; 19:614–622. [PubMed: 15005849]

[56]. Ewart L, Suresh S. Crack propagation in ceramics under cyclic loads. J Mat Sci. 1987; 22:1173–1192.

[57]. Gupta HS, Seto J, Wagermaier W, Zaslansky P, Boesecke P, Fratzl P. Cooperative deformation of mineral and collagen in bone at the nanoscale. Proc Natl Acad Sci. 2006; 103:17741–17746. [PubMed: 17095608]

[58]. Vashishth D, Tanner KE, Bonfield W. Fatigue of cortical bone under combined axial-torsional loading. J Orthop Res. 2001; 19:414–420. [PubMed: 11398854]

[59]. Hernandez CJ, Tang SY, Baumbach BM, et al. Trabecular microfracture and the influence of pyridinium and non-enzymatic glycation-mediated collagen cross-links. Bone. 2005; 37:825–832. [PubMed: 16140600]

[60]. Tang SY, Vashishth D. Non-enzymatic glycation alters microdamage formation in human cancellous bone. Bone. 2010; 46:148–154. [PubMed: 19747573]

[61]. Engsig MT, Chen QJ, Vu TH, Pedersen AC, Therkidsen B, Lund LR, et al. Matrix metalloproteinase 9 and vascular endothelial growth factor are essential for osteoclast recruitment into developing long bones. J Cell Biol. 2000; 151:879–889. [PubMed: 11076971]

[62]. Rasmussen P. Calcium deficiency, pregnancy, and lactation in rats. Microscopic and microradiographic observations on bones. Cal Tis Res. 1977; 23:95–102.

[63]. Wong KM, Singer L, Ophaug RH, Klein L. Effect of lactation and calcium deficiency, and of fluoride intake, on bone turnover in rats: isotopic measurements of bone resorption and formation. J Nutr. 1981; 111:1848–1854. [PubMed: 7288507]

[64]. Wong KM, Singer L, Ophaug RH. Effect of lactation and/or calcium deficiency on cyclic-AMP production and bone enzyme activities in rats: lack of effect of long-term fluoride administration. Ann Nutr Metab. 1983; 27:125–131. [PubMed: 6303199]

[65]. Haller AC, Zimny ML. Effects of hibernation on interradicular alveolar bone. J Dent Res. 1977; 56:1552–1557. [PubMed: 277478]

[66]. Steinberg B, Singh IJ, Mitchell OG. The effects of cold-stress. Hibernation, and prolonged inactivity on bone dynamics in the golden hamster, Mesocricetus auratus. J. Morphol. 1981; 167:43–51. [PubMed: 7241597]

[67]. Harvey KB, Donahue SW. Bending properties, porosity, and ash fraction of black bear (Ursus americanus) cortical bone are not compromised with aging despite annual periods of disuse. J Biomech. 2004; 37:1513–1520. [PubMed: 15336926]

[68]. Qing H, Ardeshirpour L, Pajevic PD, et al. Demonstration of Osteocytic Perilacunar/Canalicular Remodeling in Mice during Lactation. J Bone Mineral Research. 2012 DOI 10.1002/jbmr.1567.

[69]. Liu XS, Ardeshirpour L, VanHouten JN, et al. Site-Specific Changes in Bone Microstructure, Mineralization, and Stiffness during Lactation and After Weaning in Mice. J Bone Mineral Research. 2012 DOI 10.1002/jbmr.1503.

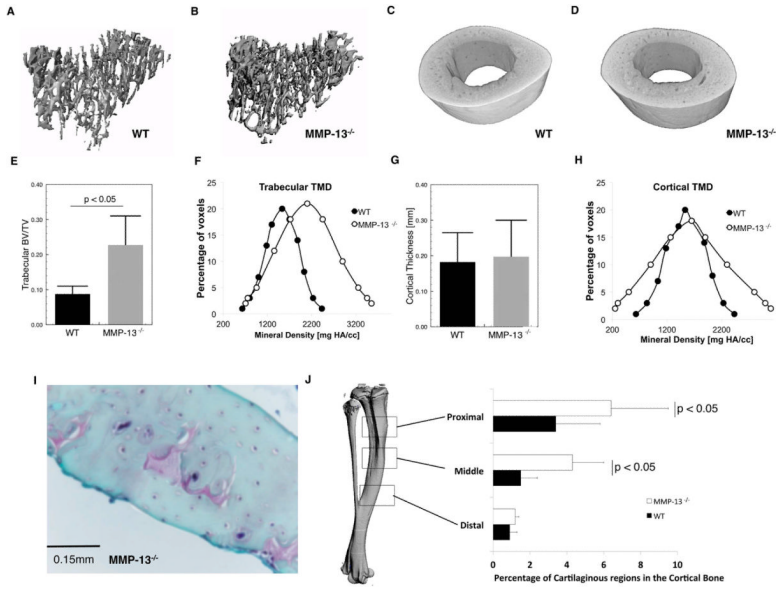

Figure 1. MMP-13-deficiency results in increased trabecular bone volume and the altered distribution cortical bone mineralization

The trabecular bone contoured from the proximal region of the tibia confirms previous observations that MMP-13$^{-/-}$ bones have significantly increased trabecular bone volume fraction (BV/TV; $p < 0.05$) (A, B, E, F). MMP-13-deficiency did not affect the geometric structure of the cortical bone (cortical thickness; $p = 0.52$) (C, D, G). Nonetheless, a histographic plot of the cortical bone tissue mineral densities (Cortical TMD) reveals that MMP-13$^{-/-}$ mice have significantly altered TMD distribution ($p < 0.001$), characterized by an increased incidence of lower and higher TMD compared to the WT (H). This can in part be explained by the osteoid remnants, which stain red with Safranin-O, that are predominantly observed in the middle and proximal aspects of the tibia (I). However there were no detectable differences in Safranin-O staining in the distal region near the tibiofibular junction where bulk of the subsequent analyses were performed (J).

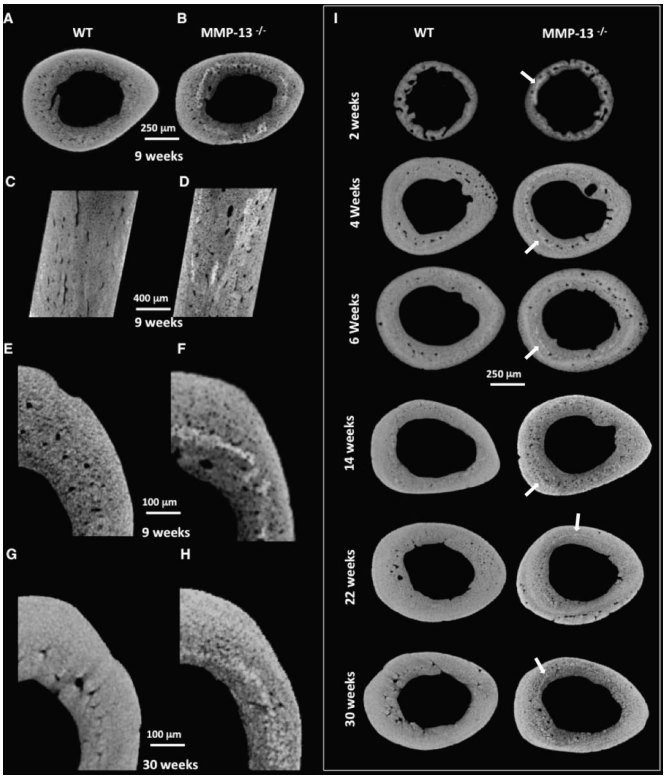

Figure 2. Hypermineralization of MMP-13-deficient mid-cortical bone matrix occurs through development and persists though aging

The incidence of higher TMD in the two-month old animals observed in the mineral distribution histogram (Figure 1H) can be visualized in images obtained from high-resolution micro-computed tomography (A – F). The increased mineralization heterogeneously localizes to the mid-cortical regions of the MMP-13$^{-/-}$ bones (E, F). These highly attenuating mineral bands appear throughout the longitudinal sections of MMP-13-deficient bone (C, D). Using high-resolution x-ray tomographic microscopy to examine developing bone (2-, 4-, and 6- weeks old) as well as aging bone (14-, 22-, and 30- weeks old), we found that this hypermineralization can be observed as early as 2 weeks of age (I) and persists for at least 30 weeks (G, H, I). Throughout growth, the band of hypermineralization in MMP-13$^{-/-}$ bone (arrowheads) is maintained approximately midway between the periosteal and endosteal surfaces.

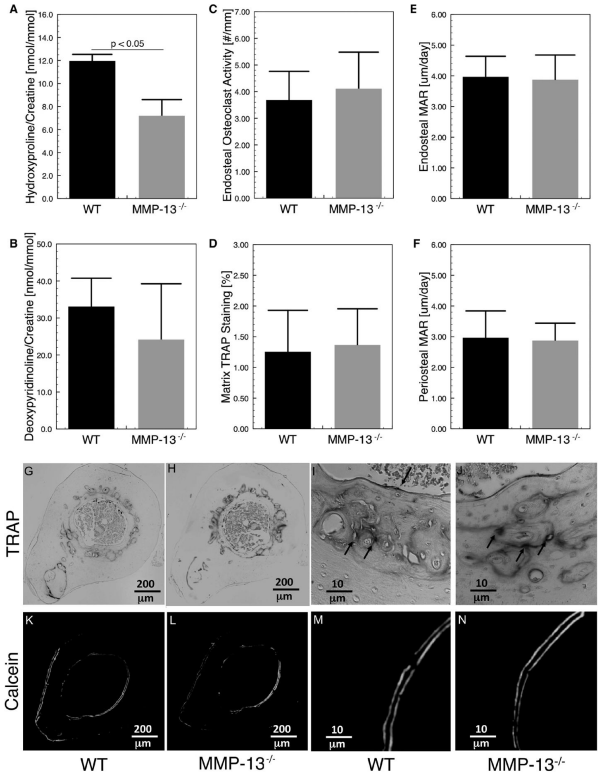

Figure 3. Conventional measures of bone formation and resorption are normal in MMP-13-deficient mice

Global deficiency of MMP-13 resulted in reduced overall tissue turnover, as shown by reduced urinary hydroxyproline ($p < 0.05$), (A); but urinary deoxypyridinoline (DPD), a crosslink specific to bone resorption, was not significantly affected ($p = 0.09$), (B). Two measures of osteoclast activity, endosteal osteoclast number (C) and tartrate resistant acid phosphatase (TRAP) positive matrix (D), reveal no differences in the expression and activation of osteoclasts between the two groups (G, H, I, J). Dynamic histomorphometric analyses (K, L, M, N) show that endosteal and periosteal matrix apposition rate (MAR), (E, F), two parameters of bone formation, are not affected by MMP-13-deficiency.

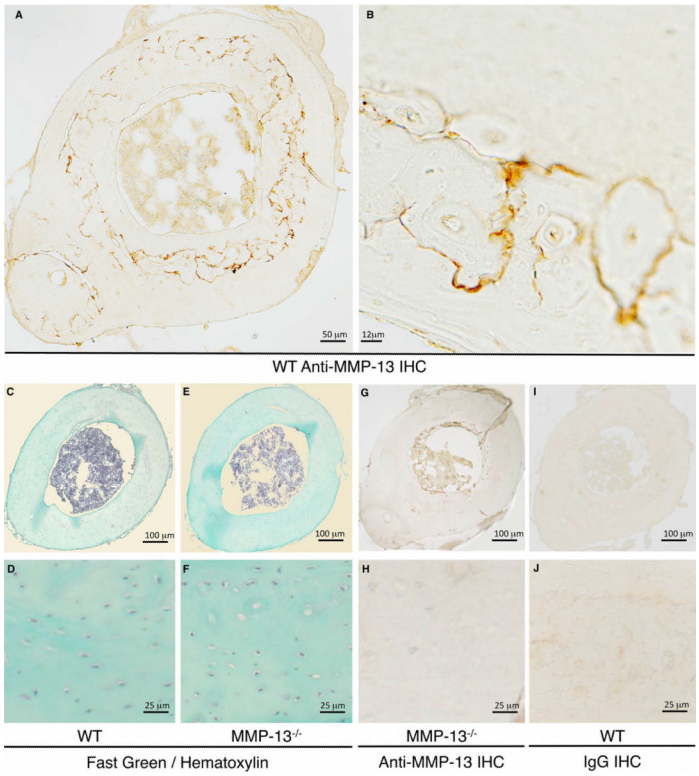

Figure 4. MMP-13 preferentially localizes to the mid-cortex of cortical bone

Immunohistochemistry (IHC) for MMP-13 shows specific staining (dark stain) in WT (A, B), but not in MMP-13-deficient (G, H), cortical bone. Fast Green and hematoxylin stained paraffin cross-sections of tibial bone reveal no notable differences in bone morphology between WT and MMP-13$^{-/-}$ mice (C, D, E, F). Controls in which primary antibody was replaced with immunoglobulin (IgG) further confirm the specificity of the MMP-13 IHC (I, J).

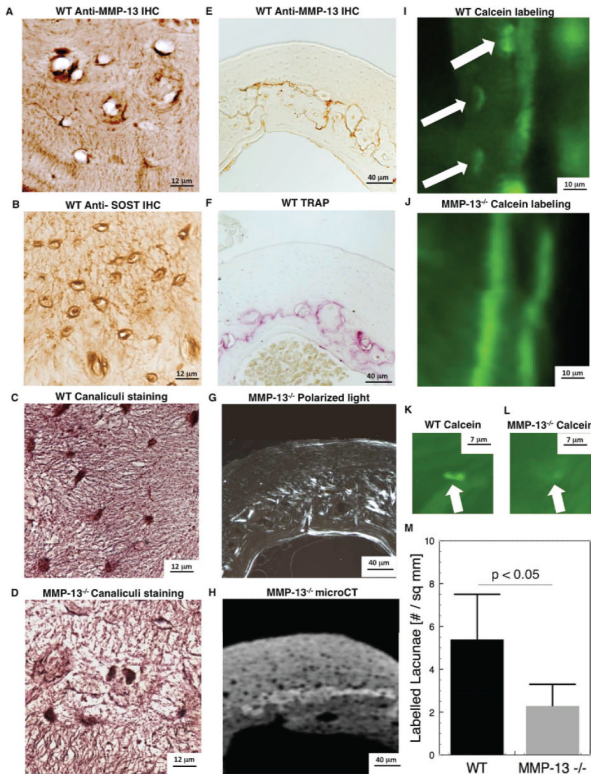

Figure 5. MMP-13 is required for normal osteocyte perilacunar matrix remodeling in mid-cortical bone

IHC staining for MMP-13 (A) and SOST (B) show osteocyte lacunar and canalicular localization of both proteins in WT tibial cortical bone. Thionin staining shows that the normal canalicular organization of mid-cortical bone is disrupted by MMP-13 deficiency (C, D). MMP-13 localization in mid-cortical WT bone (E) overlaps with TRAP-staining in WT bone (F). Loss of MMP-13-mediated matrix remodeling by osteocytes causes collagen (G) and mineralization (H) defects in the same region of mid-cortical bone. Calcein-labeling of osteocyte lacunae near the periosteal surface (I) or in the mid-cortical region (K) of WT bone was less intense and less frequent in MMP-13$^{-/-}$ bone (J, L, M).

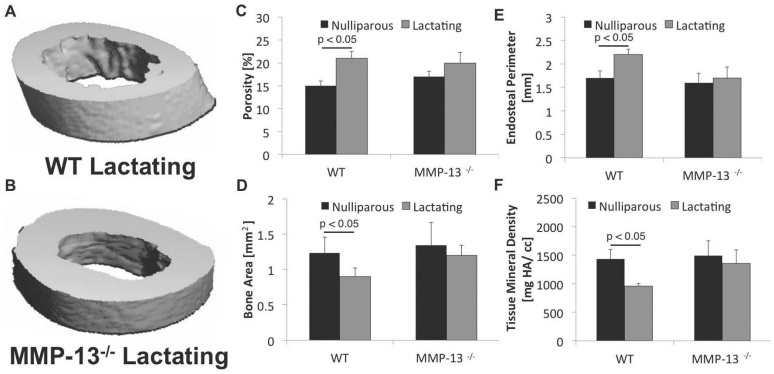

Figure 6. MMP-13 is required for lactation-induced bone loss

MicroCT analysis of tibia from nulliparous and lactating WT show that lactation causes significant increases in cortical bone porosity (C; $p < 0.05$; t-test) and endosteal perimeter (E; $p < 0.05$; t-test), and decreases in cortical bone area (D; $p< 0.05$; t-test) and tissue mineral density (F; $p< 0.05$; t-test). In contrast, the cortical bone structural parameters of MMP-13$^{-/-}$ mice, when compared to MMP-13$^{-/-}$ nulliparous controls, were not significantly altered by lactation demonstrating the need for MMP-13 for osteocyte-mediated remodeling of perilacunar matrix.

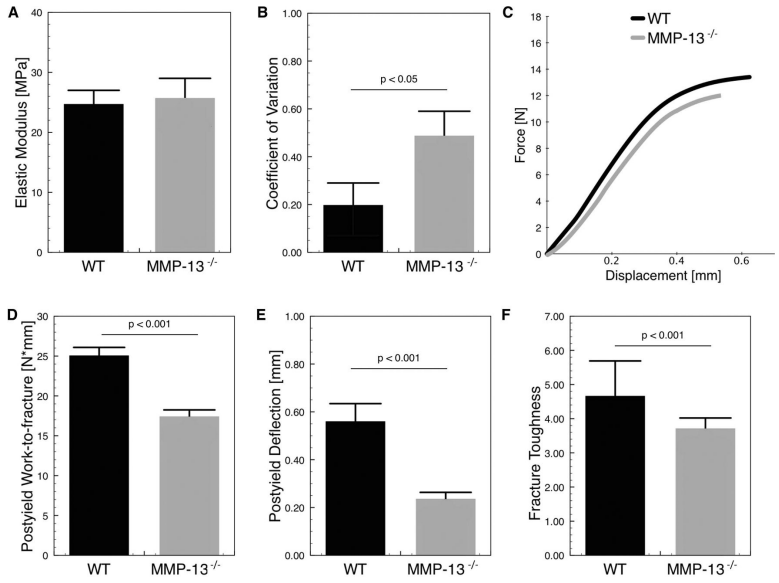

Figure 7. Impaired bone quality in MMP-13-deficient mice

Although the loss of MMP-13 did not affect the average bone matrix elastic modulus as measured by microindentation (A), the variation among MMP-13−/− mice was significantly greater than among WT mice ($p < 0.05$), (B). At the whole bone level, three-point bending tests show that MMP-13−/− bones have significantly reduced post-yield work-to-fracture ($p < 0.001$), (D) and post-yield deflection ($p < 0.001$), (E). A representative force-displacement curve of the whole bone tests confirm that the two groups primarily differ in the post-yield regions rather than elastic regions (C). Notched crack propagation tests of the whole bone also show that MMP-13-deficient bone matrix has reduced fracture toughness (F).

Table I

Structural parameters of trabecular and cortical bone as measured by microCT.

Structural parameter	Wild-type	MMP-13$^{-/-}$	p-value
Femur cortical thickness (c.Th.) [mm]	0.13 ± 0.07	0.16 ± 0.09	0.21
Femur cortical moment of inertia (c. MOI) [1/mm^4]	0.11 ± 0.05	0.13 ± 0.04	0.42
Tibia cortical thickness (c.Th.) [mm]	0.17 ± 0.09	0.21 ± 0.11	0.52
Tibia cortical moment of inertia (c. MOI) [1/mm^4]	0.13 ± 0.06	0.14 ± 0.07	0.38
Trabecular bone volume fraction (BV/TV)	**0.10 ± 0.02**	**0.22 ± 0.08**	**< 0.001**
Trabecular structure model index (SMI)	**1.7 ± 0.54**	**2.3 ± 0.32**	**< 0.01**
Trabecular tissue mineral density (tTMD)	**1323 ± 432**	**2386 ± 873**	**< 0.05**
Trabecular connectivity (t. Conn.)	143 ± 45	162 ± 54	0.33

Significant values are noted in bold.

Table II

Mechanical properties at the whole bone and tissue (fracture toughness) levels.

Mechanical property	Wild-type	MMP-13$^{-/-}$	p-value
Structural stiffness [N/mm]	134 ± 14.9	154 ± 19.5	0.82
Ultimate load [N]	0.11 ± 0.05	0.13 ± 0.04	0.77
Post-yield deflection [mm]	**0.17 ± 0.09**	**0.21 ± 0.11**	**< 0.001**
Post-yield work-to-fracture [mJ]	**24.5 ± 1.55**	**16.9 ± 1.35**	**< 0.001**
Fracture toughness [MPa√m]	**4.54 ± 0.15**	**3.59 ± 0.43**	**< 0.001**

Significant values are noted in bold.